Dynamic polarization effects in ion channeling through single-wall carbon nanotubes

Da-Peng Zhou and You-Nian Wang*
State Key Lab of Materials Modification by Beams, Department of Physics, Dalian University of Technology, Dalian, China 116023

Li Wei
Department of Physics and Computer Science, Wilfrid Laurier University Waterloo, Ontario, Canada, N2L 3C5

Z. L. Mišković
Department of Applied Mathematics, University of Waterloo, Waterloo, Ontario, Canada N2L 3G1
(Received 17 March 2005; revised manuscript received 12 May 2005; published 23 August 2005)

Ion channeling through a single-wall carbon nanotube is simulated by solving Newton's equations for ion motion at intermediate energies, under the action of both the surface-atom repulsive forces and the polarization forces due to the dynamic perturbation of the nanotube electrons. The atomic repulsion is described by a continuum potential based on the Thomas-Fermi-Moliere model, whereas the dynamic polarization of the nanotube electrons is described by a two-dimensional hydrodynamic model, giving rise to the transverse dynamic image force and the longitudinal stopping force. In the absence of centrifugal forces, a balance between the image force and the atomic repulsion is found to give rise to ion trajectories which oscillate over peripheral radial regions in the nanotube, provided the ion impact position is not too close to the nanotube wall, the impact angle is sufficiently small, and the incident speed is not too high. Otherwise, the ion is found to oscillate between the nanotube walls, passing over a local maximum of the potential in the center of the nanotube, which results from the image interaction. The full statistical analysis of 10^3 ion trajectories has been made to further demonstrate the actual effect of dynamic polarization on the ion channeling.

DOI: 10.1103/PhysRevA.72.023202 PACS number(s): 36.40.−c, 41.75.Ht, 61.82.Rx

I. INTRODUCTION

The single-wall carbon nanotube (SWNT) is a hollow cylindrical molecule with the diameter of the order of 1 nm and the length of many microns, which can be considered as a graphitic carbon plane (or graphene sheet) rolled around a cylinder [1]. Owning to their hollow structure, it would be possible to transport efficiently energetic charged particles, such as electrons and protons, through carbon nanotubes in a manner quite similar to the usual crystal channeling. In comparison with crystal channels, nanotubes can provide much longer dechanneling lengths owing to a very low electron density in their interior. Confirmation of the feasibility of channeling through nanotubes may boost some new applications, e.g., in particle accelerators, for production of nanoscale ion beams, or radiation sources of hard x rays. In particular, focused nanobeams could find applications in biological studies and medical therapy.

During the past several years, significant progress has been achieved in theoretical investigation of the transport of fast charged particles through carbon nanotubes. The first study was conducted by Klimov and Letokhov [2], who demonstrated the possibility of hard x-ray generation by relativistic charged particles channeled inside SWNTs. This work was soon followed by Gevorgian *et al.* [3] who calculated the profile of the atomic potential for SWNT ropes, and studied analytically the channeling trajectories of relativistic protons inside a SWNT. Short thereafter, Dedkov [4] investigated the possibility of transporting different types of radiation and high-energy particle beams through SWNTs. Almost at the same time, Zhevago and Glebov [5] calculated the spectra of electromagnetic radiation accompanying the channeling of relativistic charged particles through the straight and bent nanotubes. In the more recent studies, several groups have used computer simulations to study additional aspects of charged particle channeling through the ropes of SWNTs, such as the onset of dynamical chaos in ion scattering at nanotube walls [6], the possibility of extracting nanobeams from particle accelerators using bent nanotube ropes [7], the effects of incoherent scattering on channeling trajectories [8], and the rainbow effect in proton channeling through short nanotube ropes [9]. Quite recently, channeling of relativistic particles through isolated multiwalled carbon nanotubes (MWNT) was also studied [10].

In all the above studies, the nanotube wall potential was calculated in the continuous model, either as the average along both the axis and the circumference of the wall for chiral nanotubes [2–5,7,10], or as a stack of continuous atomic rows in the walls of the armchair and zigzag nanotubes [5,6,8,9]. While the above studies of channeling through carbon nanotubes considered *high-energy* particles (with energies typically ranging from MeV to GeV), there are only few accounts of the particle transport at low energies (typically keV and under) [11,12]. In those, Dedkov analyzed various forces on low-energy ions and neutral atoms moving through SWNTs using the continuous potential model [11], whereas Krashenninikov and Nordlund used atomistic simulation based on the molecular dynamics method to study the channeling of keV argon ions through MWNTs [12].

*Email address: ynwang@dlut.edu.cn

One should note that, at *high* ion energies, the effects of the dynamic polarization of the nanotube electrons on ion trajectories are negligible, so that the ion channeling is predominantly governed by the repulsive force due to elastic scattering at carbon atoms in the nanotube walls. On the other hand, at *low* ion energies, the energy losses to single electron excitations are usually negligible in the interior regions of nanotubes due to very low electron densities, whereas the energy losses at the nanotube walls are dominated by the nuclear stopping [11,12]. In addition, some low-energy ions are efficiently neutralized at the nanotube wall, so that the polarization interaction with the nanotube electrons, or the image interaction, is not expected to play significant role in channeling, although dynamical van der Waals interaction could be important for neutral particles close to the nanotube walls [11]. However, it has been shown recently by Arista [13] that the dynamic polarization of the surrounding dielectric medium can strongly affect the motion of ions through cylindrical channels and microcapillaries in solids at intermediate energies (in the range from keV to MeV). Apparently, up to now, there were no reports on analyzing the ion channeling through carbon nanotubes at such energies.

It has been shown recently that, at the intermediate ion energies, collective excitations of the nanotube electrons give rise to substantial energy losses, as well as to strong dynamic-image interaction, for ions moving inside or outside of both SWNTs [14–16] and MWNTs [17], parallel to their axes. The significance of such interactions has been recently demonstrated through a theoretical prediction of the existence of tubular electron image states around SWNTs [18] and subsequent experimental confirmation of such states [19]. It is expected that, in ion channeling through carbon nanotubes, the dynamical image interaction will exert a strong radial force which attracts the ions toward the nanotube wall. While this effect is certainly absent in the conventional channeling through crystal targets, it has been neglected in the previous studies of ion channeling through carbon nanotubes. Therefore, a purpose of the present article is to elucidate the effects of dynamic polarization of the nanotube electrons, described by a two-dimensional (2D) hydrodynamic model [14–17], on the trajectories of fast ions channeled through single SWNTs, where the repulsive continuum potential of the nanotube wall is obtained from the Thomas-Fermi-Moliere model atomic potential [3,4,6,9]. In Sec. II, trajectories of nonrelativistic charged particles inside a SWNT are determined by solving the equations of motion, whereas the numerical results are presented and discussed in Sec. III for a range of the incident projectile parameters. Concluding remarks are given in Sec. IV. Atomic units (a.u.) are used throughout, unless otherwise indicated.

II. EQUATIONS OF MOTION

Consider a nonrelativistic ion with mass M, incident at the open end of a straight SWNT with velocity $\mathbf{v}_0$ under small angle θ_0 relative to the nanotube axis. The nanotube wall is represented by an infinitely long cylindrical shell of radius a on which carbon atoms form infinitesimally thin jellium with the surface density $n_{sa}=0.1063$. The four valence electrons per carbon atom are considered to form a free-electron gas distributed uniformly over the cylindrical surface, with the density per unit area $n_0=4n_{sa}$, corresponding to a graphene sheet [20]. The equations of motion for the cylindrical coordinates (ρ,ϕ,z) of the projectile ion are

$$M\ddot{\rho}=F_{\rho}^{(n)}+F_{\rho}^{(p)}+\frac{L_0^2}{M\rho^3}, \tag{1}$$

$$M\ddot{z}=F_{z}^{(p)}, \tag{2}$$

$$M\rho^2\dot{\phi}=L_0, \tag{3}$$

where $F_{\rho}^{(n)}$ is the repulsive radial force produced by the surface continuum potential $\mathbf{F}^{(p)}=\{F_{\rho}^{(p)},F_{z}^{(p)}\}$ is the dynamic polarization force due to the excitations of the electron gas, and L_0 is the ion angular momentum relative to the nanotube axis, which is conserved due to the axial symmetry of the forces involved. The last term in Eq. (1) represents the centrifugal force which may strongly deflect the ion trajectory towards the nanotube wall, depending on the magnitude of the angular momentum $L_0=M\rho_0 v_0 \sin\phi_0 \sin\theta_0$ acquired at the impact point (ρ_0,ϕ_0,z_0) in the entrance cross section of the nanotube at $z_0=0$. On the other hand, we stress that all previous studies of ion channeling through carbon nanotubes neglected both the dissipative part $F_{z}^{(p)}$ and the conservative part $F_{\rho}^{(p)}$ of the polarization force [2–10]. Consequently, in order to elucidate the effects of these forces, we consider here only the cases where the incident plane of the ion passes through the nanotube axis ($\phi_0=0$), so that $L_0=0$, and the centrifugal force in Eq. (1) can be discarded hereafter.

We use Thomas-Fermi-Moliere's approximation for the interaction potential between a point-charge particle (representing a completely stripped ion) and an individual carbon atom in the nanotube surface [4]. After averaging over the polar angle and the longitudinal coordinate (ϕ,z) one obtains the continuum potential as follows:

$$U_n(\rho)=4\pi a n_{sa} Z_1 Z_2 \sum_{i=1}^{3} c_i I_0(b_i\rho_</d) K_0(b_i\rho_>/d), \tag{4}$$

where $\rho_<=\min(\rho,a)$ and $\rho_>=\max(\rho,a)$, Z_1 and $Z_2=6$ are the atomic numbers of the projectile and the carbon atom, respectively, $d=0.8853Z_2^{-1/3}$ is the screening length, and I_0 and K_0 are the zeroth-order modified Bessel functions. Thus, the repulsive force on the ion *inside* the nanotube is given by

$$F_{\rho}^{(n)}=-\frac{\partial U_n(\rho)}{\partial\rho}=-4\pi a/d n_{sa} Z_1 Z_2 \sum_{i=1}^{3} c_i b_i I_1(b_i\rho/d) K_0(b_i a/d), \tag{5}$$

where $I_1(x)$ is the first-order modified Bessel function. This force will efficiently repel the incident ion away from the nanotube surface.

In our previous works [14,15], we have used a linearized 2D hydrodynamic model to describe the collective electronic excitations of a SWNT, caused by a point charge Z_1 moving at a constant speed v, parallel to the nanotube axis, at a fixed

radial distance ρ. In particular, the transverse dynamic polarization force can be expressed by means of the ion self-energy (or the image potential) $E_s(\rho,v)$ as follows:

$$F_\rho^{(p)}(\rho,v) = -\frac{\partial E_s(\rho,v)}{\partial \rho} = -\frac{2Z_1^2}{\pi}\sum_{m=-\infty}^{\infty}\int_0^\infty dk\, kI_m(k\rho)I_m'(k\rho)\mathrm{Re}[A_m(k,kv)], \tag{6}$$

while the longitudinal polarization force is related to the stopping power $S(\rho,v)$ via

$$F_z^{(p)}(\rho,v) = -S(\rho,v) = \frac{2Z_1^2}{\pi}\sum_{m=-\infty}^{\infty}\int_0^\infty dk k I_m^2(k\rho)\mathrm{Im}[A_m(k,kv)], \tag{7}$$

where the auxiliary function $A_m(k,\omega)$ is given by

$$A_m(k,\omega) = \frac{\Omega_p^2 a^2(k^2+m^2/a^2)K_m^2(ka)}{\omega(\omega+i\gamma)-\omega_m^2(k)}, \tag{8}$$

with the plasmon dispersion

$$\omega_m(k) = \sqrt{(k^2+m^2/a^2)[\alpha+\Omega_p^2 a^2 K_m(ka)I_m(ka)]+\beta(k^2+m^2/a^2)^2}. \tag{9}$$

Here, $\Omega_p=(4\pi n_0/a)^{1/2}$, $\alpha=v_F^2/2$ is the square of the speed of propagation of the density disturbances in the 2D electron gas [with $v_F=(2\pi n_0)^{1/2}$ being the Fermi speed], $\beta=1/4$, and γ is a damping constant. Damping physically originates from the momentum losses of the excited electrons due to scattering on ion cores in the nanotube wall. In the absence of reliable empirical data for γ, one could take the idealized model with $\gamma\to 0^+$, but we choose the finite value $\gamma=0.01\Omega_p$ to avoid numerical inconveniences in executing the integral in Eq. (6).

We show in Fig. 1 the dependences of (a) self-energy E_s and (b) stopping power S on radial position ρ and speed v for a proton ($Z_1=1$) moving parallel to the axis of the nanotube with radius $a=20$. It can be seen that the magnitude of E_s monotonically increases with ρ while its dependence on v passes through broad minima at intermediate speeds. Stopping power S gives the energy loss per unit path length in the longitudinal direction, due to the plasmon excitations in the nanotube, which are vanishingly small below a velocity threshold of some a.u. [16,17]. Above the threshold, the stopping power passes through broad maxima at higher speeds, while its magnitude increases sharply as the projectile gets closer to the nanotube wall. In Fig. 2, we show radial dependences of the total potential E_s+U_n for two groups of ion speeds, whereas Fig. 3 displays the corresponding transverse components of the total force $F_\rho^{(p)}+F_\rho^{(n)}$. It is obvious from Fig. 2 that, unlike the cases of crystal channeling, the potential well for ion channeling through a SWNT exhibits a local maximum at the center of the nanotube, owing to the image attraction toward the nanotube wall. As a result of the counteraction of the long-ranged image force and the short-ranged repulsive continuum potential, shallow minima are seen in the potential in Fig. 2 at radial distances midway between the center and the wall, which are relatively weakly dependent on the ion speed, as documented in Fig. 3.

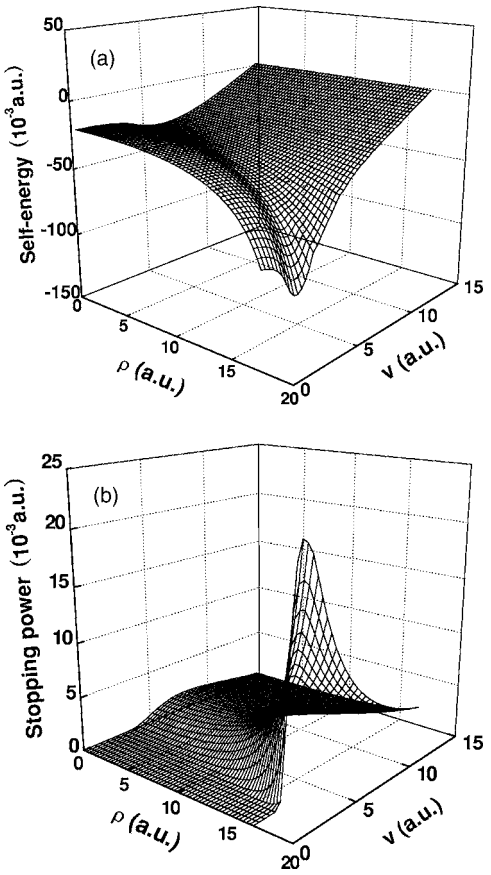

FIG. 1. (a) Self-energy E_s (in a.u.) and (b) stopping power S (in a.u.) versus radial position ρ (in a.u.) and speed v (in a.u.) for proton moving paraxially in a single-wall nanotube with radius $a=20$ a.u.

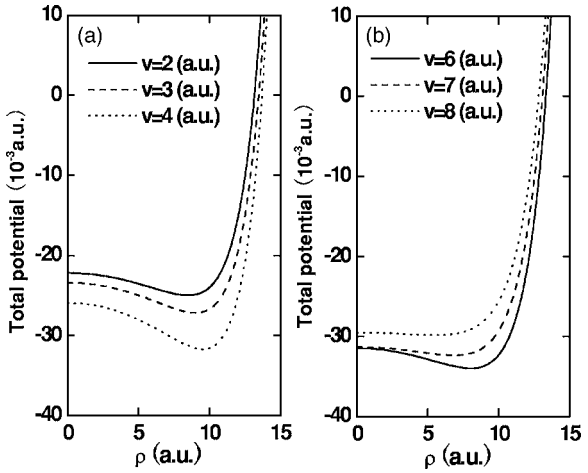

FIG. 2. Dependence of total potential E_s+U_n (in a.u.) on radial position ρ (in a.u.) for proton moving paraxially in a single-wall nanotube with radius $a=20$ a.u., at several speeds: (a) $v=2$, 3, 4 and (b) $v=6$, 7, and 8 a.u.

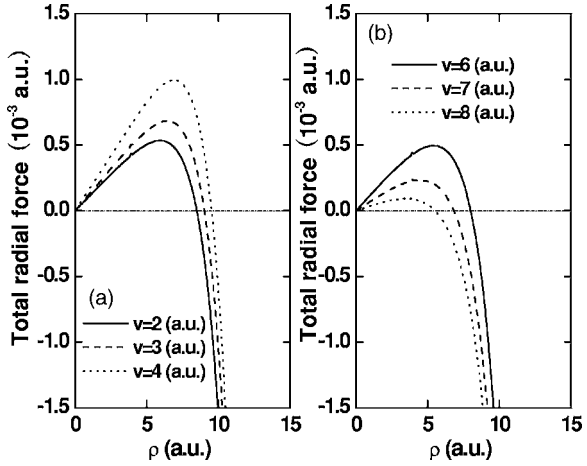

FIG. 3. Dependence of total radial force $F_\rho^{(p)}+F_\rho^{(n)}$ (in a.u.) on radial position ρ (in a.u.) for proton moving paraxially in a single-wall nanotube with radius $a=20$ a.u., at several speeds (a) $v=2$, 3, 4 and (b) $v=6$, 7, and 8 a.u.

III. NUMERICAL RESULTS

Given the initial position $\mathbf{r}_0=(\rho_0,\phi_0,z_0)$ and the initial velocity $\mathbf{v}_0=(v_0\sin\theta_0,0,v_0\cos\theta_0)$, one can determine the charged particle trajectories in a nanotube by solving Eqs. (1)–(3) numerically. In the following calculations, we take the initial longitudinal position to be $z_0=0$ and assume that the polar angle is $\phi_0=0$, corresponding to the case of ion incidence in a plane passing through the nanotube axis. Thus, the initial radial position ρ_0, the initial speed v_0, and the initial angle θ_0 are variable input parameters.

Figures 4(a)–4(d) show proton trajectories for several initial speeds, with $\rho_0=8$ and $\theta_0=0$ kept fixed, in a carbon nanotube with $a=20$. We compare in Fig. 4 the trajectories obtained with and without the dynamical polarization force.

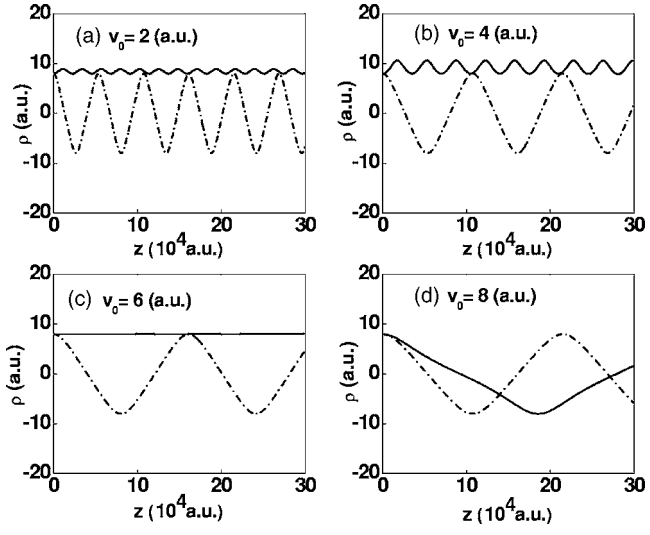

FIG. 4. Proton trajectories in a single-wall carbon nanotube with radius $a=20$ a.u. at fixed initial radial position $\rho_0=8$ a.u. and incident angle $\theta_0=0$, for several incident speeds: $v_0=2$, 4, 6, and 8 a.u. The solid and the dashed lines correspond to numerical results with and without the dynamic polarization effect, respectively.

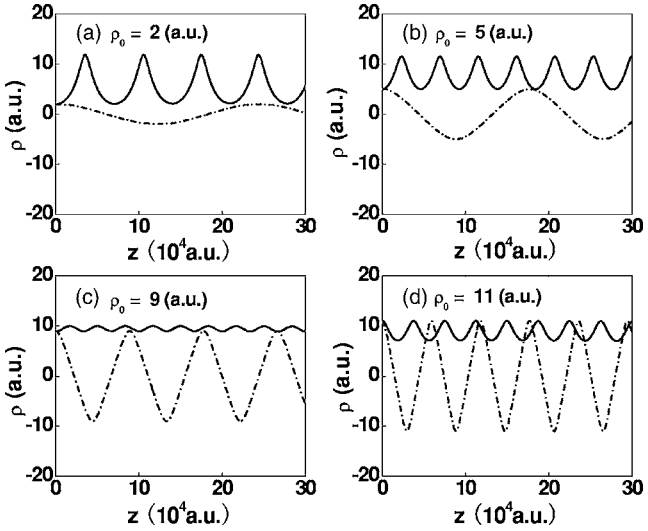

FIG. 5. Proton trajectories in a single-wall carbon nanotube with radius $a=20$ a.u. at fixed initial speed $v_0=4$ a.u. and incident angle $\theta_0=0$, for several initial radial positions $\rho_0=2$, 5, 9, and 11 a.u. The solid and the dashed lines correspond to numerical results with and without the dynamic polarization effect, respectively.

It is obvious that, if only the repulsive force is taken into account, the particle trajectories oscillate with the amplitude $\rho_{\max}=8$ and the longitudinal period Λ_z roughly proportional to the ion speed, just as in the simple harmonic-potential models of planar channeling in crystals. However, when the dynamic polarization force is included, both the oscillation amplitude and the longitudinal period are significantly smaller. In particular, the ion trajectories are seen to remain localized in the peripheral regions of radial distances above the potential wells displayed in Fig. 2, in the cases when the image force is strong enough, shown in parts (a) and (b) of Fig. 4. This localization is best illustrated in the extreme case of a straight trajectory in part (c) of Fig. 4, where the impact radial distance matches the minimum of the potential at the speed $v_0=6$, see Fig. 2. On the other hand, the image force is weaker at higher speeds, such as $v_0=8$ used in part (d) of Fig. 4, thus allowing the ion to execute large-amplitude oscillations flying over the maximum of the potential in the center of the well caused by the image attraction, shown in Fig. 2. In this case, the longitudinal period is longer than the period of a quasiharmonic trajectory in the case when the image potential is absent, and a delay of the oscillation is clearly seen in part (d) of Fig. 4, when the ion flies over the central potential hump.

Figure 5 shows the influence of the initial radial position ρ_0 on proton trajectories with fixed impact speed $v_0=4$ and initial angle $\theta_0=0$. The effect of the image force is most pronounced for impact positions close to the center of the nanotube, shown in parts (a) and (b) of Fig. 5, where the ion executes rather asymmetric oscillations in peripheral regions, characterized by sharp bouncing at the nanotube wall, which are quite different from the small-amplitude quasiharmonic oscillations about the center in the case when the image interaction is absent. The cases (c) and (d) in Fig. 5 are similar to those shown parts (a) and (b) of Fig. 4, where the particle undergoes small-amplitude oscillations around the peripheral

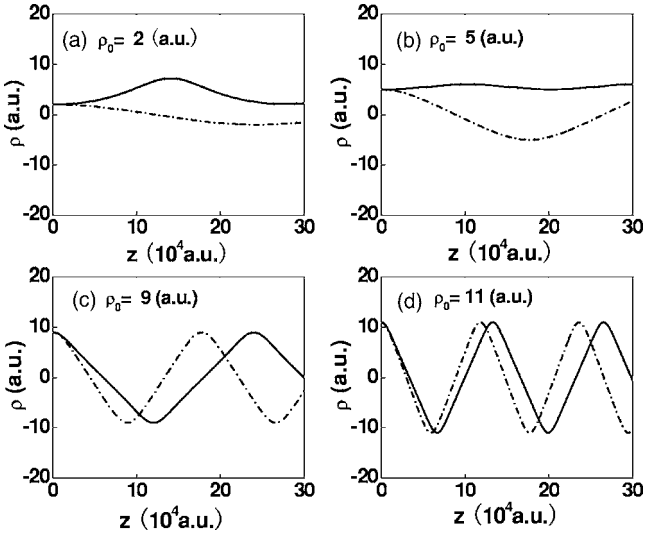

FIG. 6. Proton trajectories in a single-wall carbon nanotube with radius $a=20$ a.u. at fixed initial speed $v_0=8$ a.u. and incident angle $\theta_0=0$, for several initial radial positions $\rho_0=2$, 5, 9, and 11 a.u. The solid and the dashed lines correspond to numerical results with and without the dynamic polarization effect, respectively.

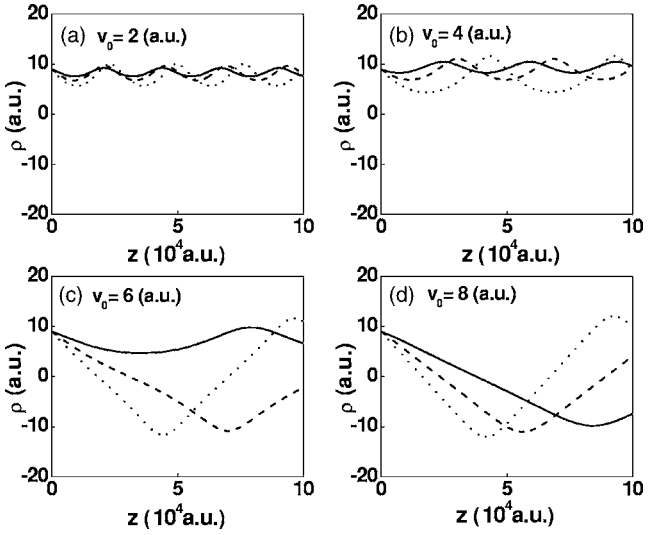

FIG. 7. Proton trajectories in a single-wall carbon nanotube with radius $a=20$ a.u. at fixed initial radial position $\rho_0=9$ a.u., for several incident speeds $v_0=2$, 4, 6, and 8 a.u. Here, the solid, dashed, and dotted lines correspond to numerical results, obtained with the polarization effects included, for incident angles $\theta_0=0.01°$, 0.02°, and 0.03°, respectively.

minima of the total potential shown in Fig. 2. In Fig. 6 we also display the influence of various initial radial positions ρ_0 on proton trajectories with fixed initial angle $\theta_0=0$, but with the higher impact speed $v_0=8$ than in Fig. 5, so that the image forces are weaker than those used in Fig. 5. The trajectories with lower impact radial positions are again localized away from the center and are governed by small-amplitude, long-period oscillations, whereas the larger impact distances allow the ion to oscillate over the center of the nanotube, similar to the case shown in part (d) of Fig. 4.

In Fig. 7 we illustrate the dependences of proton trajectories on impact angle θ_0, for several impact speeds, with $\rho_0=9$ fixed, in a nanotube with radius $a=20$. Note that only the results for full potential are displayed in Fig. 7. It is evident that the localization of oscillations above the peripheral minima of the total potential is quite persistent for all displayed angles at lower speeds, shown in parts (a) and (b) of Fig. 7, with obvious dependences of the amplitudes and the periods of oscillations on the impact angle. At higher speeds, shown in parts (c) and (d), when the image force is weaker, it is clear that increasing impact angle can switch the mode of oscillation, going from those localized in the peripheral regions to the large-amplitude oscillations over the central potential hump.

Finally, to further illustrate the dynamic polarization effect on the ion channeling, Fig. 8 shows the radial position distribution of 10^3 protons with $v_0=4$ a.u. after traveling 10^5 a.u. through the nanotube. Here the initial angles $\theta_{i0}(i=1,2,\ldots,10^3)$ are zero and the initial positions ρ_{i0} are sampled randomly from -15 to 15 a.u. It is clear that due to the dynamic polarization effect the particles localize mainly around $|\rho|=10$ a.u., which forms a "hollow beam" [see Fig. 8(a)], while the particles distribute around the center of the nanotube ($\rho=0$) if only the repulsive force is included [see Fig. 8(b)]. The results indicate again that the dynamical polarization force can attract the ions toward the nanotube wall. Similarly, we also plot in Fig. 9 the angular distribution of 10^3 protons (a) with and (b) without the dynamic polarization.

IV. CONCLUSIONS

We have simulated the channeling of medium-energy protons in single-wall carbon nanotubes by solving Newton's equations of motion, in which both the transverse and the longitudinal dynamic polarization forces are included, in ad-

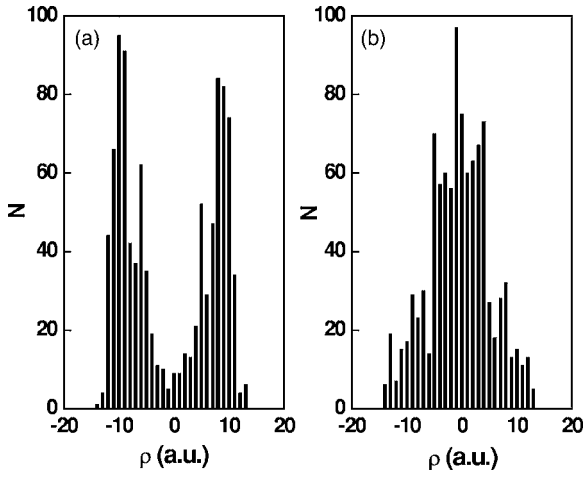

FIG. 8. The statistical distributions of the radial positions (a) with (b) without the dynamic polarization after the homogeneous beam traveled 10^5 a.u. through a single-wall carbon nanotube. Here the radius $a=20$ a.u., the initial speed $v_0=4$ a.u., the initial angles $\theta_{i0}=0$, and the initial positions ρ_{i0} are sampled randomly from -15 to 15 a.u.

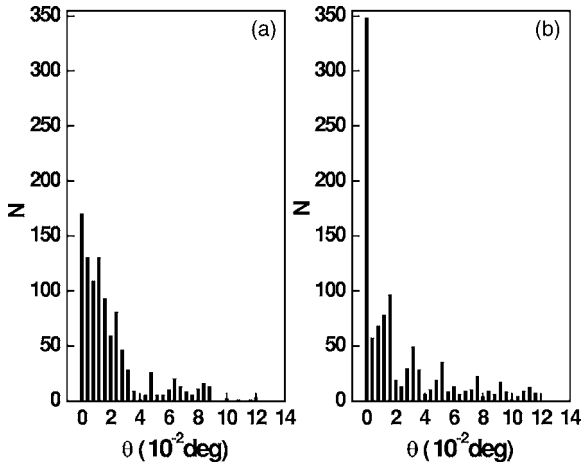

FIG. 9. The statistical distributions of the angles (a) with (b) without the dynamic polarization after the homogeneous beam traveled 10^5 a.u. through a single-wall carbon nanotube. Here the input parameters are same as those used in Fig. 8.

dition to the surface-atom repulsive forces. The polarization forces are calculated from the ion self-energy (or dynamic image potential) and the ion stopping power, described by means of a linearized 2D hydrodynamic model for the collective electron excitations in carbon nanotubes. The repulsive potential is obtained in the continuum limit by averaging the Thomas-Fermi-Moliere potential for carbon atom in the longitudinal direction and along the circumference of the nanotube wall. Given the axial symmetry of the total force, the angular momentum of ion motion through the nanotube is conserved, but we neglect the resulting centrifugal force by considering only the ion incidence in a plane passing through the nanotube axis. In such a case, it is shown that the soft transverse polarization force (or the image force) attracts the ion towards the nanotube wall, whereas the short-range continuum potential provides a strongly repulsive force when the ion approaches the wall closely. As a result, local minima in the radial dependence of the total potential arise in peripheral regions in the nanotube, at distances midway between the nanotube center and its wall. Numerical results show that proton oscillates over these peripheral regions, provided (a) the impact radial distance is not too close to the nanotube wall, (b) the impact angle relative to the nanotube axis is sufficiently small, and (c) the incident ion speed is not too high. Otherwise, the ion is found to oscillate between the nanotube walls, flying over a local maximum at the center of the nanotube, which originates from the image potential. Numerical results also indicate that the energy losses due to plasmon excitations in single-walled nanotube are negligible for nanotube lengths of some micrometer.

For further illustrating the importance of the dynamic polarization effect, we also present a full statistical analysis of ion trajectories, including the distributions of the radial position and angle, by simulating the passages of 10^3 ions with the random distributions of the initial positions. The results indicate that the dynamic polarization effect results in the "hollow beam" formation.

Extensions will be made to study medium-energy ion channeling through multiwalled carbon nanotubes and the nanotube ropes. In addition, a work is in progress which will use a 3D hydrodynamic model for electron excitations in the nanotube walls, which will be more consistent with the present modeling of the atomic repulsion. As mentioned in the Introduction, possible applications of ion channeling through nanotubes at intermediate energies could lead to creation of nano-beams for use in various radiation and plasma technologies, as well as in the biological studies and medical therapy.

ACKNOWLEDGMENTS

This work is supported by the National Natural Science Foundation of China (Grant No. 10275009). Z.L.M. acknowledges the supports from NSERC and PREA.

[1] S. Iijima, Nature (London) **354** 56 (1991).
[2] V. V. Klimov and V. S. Letokhov, Phys. Lett. A **222**, 424 (1996).
[3] L. A. Gevorgian, K. A. Ispirian, and R. K. Ispirian, JETP Lett. **66**, 322 (1997); Nucl. Instrum. Methods Phys. Res. B **145**, 155 (1998).
[4] G. V. Dedkov, Nucl. Instrum. Methods Phys. Res. B **143**, 584 (1998); G. V. Dedkov and B. S. Karamurzov, Surf. Coat. Technol. **128**, 51 (2000).
[5] N. K. Zhevago and V. I. Glebov, Phys. Lett. A **250**, 360 (1998).
[6] A. A. Greenenko and N. F. Shul'ga, Nucl. Instrum. Methods Phys. Res. B **193**, 133 (2002); **205**, 767 (2003).
[7] V. M. Biryukov and S. Bellucci, Phys. Lett. B **542**, 111 (2002); S. Bellucci, V. M. Biryukov, Yu. A. Chesnokov, V. Guidi, and W. Scandale, Nucl. Instrum. Methods Phys. Res. B **202**, 236 (2003); Phys. Rev. ST Accel. Beams **6**, 033502 (2003).
[8] N. K. Zhevago and V. I. Glebov, Phys. Lett. A **310**, 301 (2003).
[9] S. Petrovic, D. Borka, and N. Neskovic, Nucl. Instrum. Methods Phys. Res. B **230**, 106 (2005).
[10] S. Bellucci, V. M. Biryukov and A. Cordelli, Phys. Lett. B **608**, 53 (2005).
[11] G. V. Dedkov, Surf. Coat. Technol. **158-159**, 75 (2002).
[12] A. V. Krasheninnikov and K. Nordlund, Nucl. Instrum. Methods Phys. Res. B **228**, 21 (2005).
[13] N. R. Arista, Phys. Rev. A **64**, 032901 (2001); Nucl. Instrum. Methods Phys. Res. B **182**, 109 (2001).
[14] Y. N. Wang and Z. L. Mišković, Phys. Rev. A **66**, 042904 (2002); **69**, 022901 (2004).
[15] D. J. Mowbray, Z. L. Miskovic, F. O. Goodman, and Y.-N. Wang, Phys. Lett. A **329**, 94 (2004).
[16] D. J. Mowbray, Z. L. Miskovic, F. O. Goodman, and Y.-N. Wang, Phys. Rev. B **70**, 195418 (2004).
[17] D. J. Mowbray, S. Chung, Z. L. Miskovic, F. O. Goodman, and

Y.-N. Wang, Nucl. Instrum. Methods Phys. Res. B **230**, 142 (2005).

[18] B. E. Granger, P. Kral, H. R. Sadeghpour, and M. Shapiro, Phys. Rev. Lett. **89**, 135506 (2002).

[19] M. Zamkov, N. Woody, B. Shan, H. S. Chakraborty, Z. Chang, U. Thumm, and P. Richard, Phys. Rev. Lett. **93**, 156803 (2004).

[20] D. Ostling, D. Tomanek, and A. Rosen, Phys. Rev. B **55**, 13 980 (1997).